CONTRIBUTED PAPER

Key Issues With Printed Flexible Thin Film Transistors and Their Application in Disposable RF Sensors

This paper outlines why hybrid printing processes for fabricating flexible organic thin film transistors is not transferrable to fully scalable printing processes because of threshold voltage (V_{th}) variations.

By Jinsoo Noh, Minhoon Jung, Younsu Jung, Chisun Yeom, Myoungho Pyo, and Gyoujin Cho, *Member IEEE*

ABSTRACT | This paper addresses the key issues that must be overcome to realize fully printed TFT-based flexible devices *via* commercially viable methods. In particular the threshold voltage (V_{th}) variation in printed TFTs is a serious impediment to the successful launch of fully printed TFT-based devices in the market. The underlying causes of the V_{th} variation in fully printed TFTs were analyzed by considering the misalignment of printed drain-source to gate electrodes, the rheology of electronic inks and effects from external sources of charge. By alleviating the influences of external sources of charge using a printed passivation layer, V_{th} variation is maintained below 30% using a fully printed process. Based on the attainable variation range, the required number of integrated TFTs was estimated to fabricate a fully printed TFT-based radio frequency (RF) sensor device. A practical compromise enables fully printed RF sensors to be realized *via* the scalability of printing processes that mitigate V_{th} variation by minimizing the level of TFT integration. Prototypes of fully printed RF sensors with human interactive capability—an RF sensor label, and an RF *e*-sensor (cyclic voltammetry) tag—are enabled with as few as 26 printed TFTs, demonstrating that low-cost and high throughput manufacturing of printed electronics is feasible.

KEYWORDS | Printed electronics; printed radio frequency (RF) *e*-sensors; printed radio frequency sensors; printed thin film transistor

I. INTRODUCTION

Printed electronics, especially for manufacturing fully printed thin film transistor (TFT)-based devices, is considered an innovative technology in the IT (Information technology) industry. However, practical realization of this technology remains elusive because printing processes cannot achieve comparable printed TFT structures to those fabricated using vacuum deposition and photolithographic processes (Fig. 1). Surface roughness of printed layers, edge waviness of the patterns, and poor registration accuracy of the drain-source electrodes to the gate electrode generates a wider range of threshold voltage (V_{th}) variation in the printed TFTs compared to TFTs fabricated using hybrid processes utilizing the vacuum deposition and photolithographic processes. As the V_{th} variation in TFTs becomes larger, fewer opportunities exist to fabricate commercially relevant integrated devices.

In this article, we describe the key issues causing the V_{th} variation that are impeding the successful deployment of printed TFT-based devices in Information Technology (IT) markets and provide a strategy to resolve them. We

Manuscript received September 16, 2014; revised December 27, 2014 and February 21, 2015; accepted February 25, 2015. Date of current version May 19, 2015. This work was supported by the RIC of Sunchon National University and the Basic Science Research Program through the National Research Foundation of Korea (NRF) funded by the Ministry of Education (NRF-2014R1A6A1030419). J. Noh, M. Jung, and Y. Jung equally shared the first authorship. *(Corresponding author: G. Cho.)*

J. Noh, **Y. Jung**, **C. Yeom**, **M. Pyo**, and **G. Cho** are with the Department of Printed Electronics Engineering, Sunchon National University, Suncheon, Jeonnam 540-742, Korea (e-mail: njinsoo@hanmail.net; isinu7@naver.com; chtjsdml21@naver.com; mho@sunchon.ac.kr; gcho@sunchon.ac.kr).

M. Jung is with the Printed Electronics Research Institute, PARU Co. Seomyeon, Suncheon, Jeonnam 540-742, Korea (e-mail: jungminhun@gmail.com).

Digital Object Identifier: 10.1109/JPROC.2015.2410303

0018-9219 © 2015 IEEE. Translations and content mining are permitted for academic research only. Personal use is also permitted, but republication/redistribution requires IEEE permission. See http://www.ieee.org/publications_standards/publications/rights/index.html for more information.

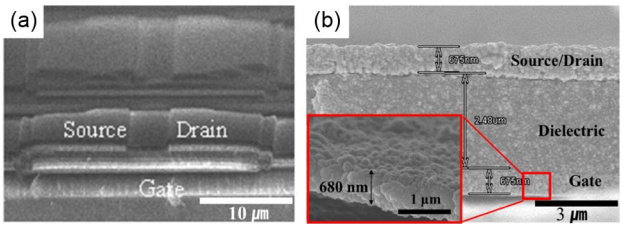

Fig. 1. *Basic structure of a bottom-gate thin film transistor (TFT) using photolithography with (a) vacuum deposition (Electron Lett. vol. 41, no. 14, pp. 822-823, 2005) and (b) all printed processes. Cross-sectional SEM image of an all printed TFT shows nonuniform structures at the interfaces between printed layers.*

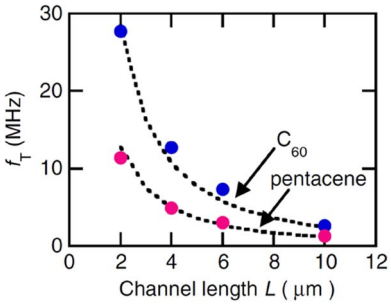

Fig. 2. *Plot of the channel-length dependency on the cutoff frequency of TFTs based on C_{60} and pentacene [7].*

begin by first outlining the issues limiting the implementation of fully printed TFT devices in generic terms to situate the reader before providing specific solutions that will enable commercial manufacturing of fully printed TFT-based devices.

General introduction: Currently, there exists unsubstantiated hope in the scientific community and industry that fully printed TFT-based flexible electronic devices will soon emerge and drastically change everyday life [1]–[4]. The big advantage of employing printed TFTs over current Si-based TFTs is scalability and an extremely low manufacturing cost [5] for disposable and human interactive flexible IT devices. However, we are often misled into expecting printed TFTs will reach comparable performance to Si-based TFTs that can interface with current Si-based highly functional devices such as smartphones and tablet PCs. This is why researchers set a goal to develop semiconducting inks to print TFTs with mobility similar to Si [6] where an operation frequency of integrated logic circuits is usually higher than 100 kHz at a short channel length ($< 10\ \mu$m). However, since current printing technology is far from being able to fabricate short channel TFTs ($< 10\ \mu$m), fully printed TFT-based logic devices (not a single TFT) with 100 kHz operating frequencies cannot be manufactured. In large part, this is due to misalignment of printed drain and source electrodes with the gate electrode. The channel length dependence of the operation frequency (f_T) for two semiconductors with similar charge mobility (pentacene and C_{60}) is shown Fig. 2 [7]. In fact, the channel length is a dominant factor in f_T of TFTs as shown in the equation: $f_T \approx u_{\text{eff}}(V_{\text{GS}} - V_{\text{th}})/2\pi L(L + 2L_C)$ where u_{eff} is the effective charge-carrier mobility, L is the channel length, and L_C is the contact length [8]. L_C represents the length of overlap between drain-source electrodes and gate electrode. Therefore, a short channel length with precisely aligned drain-source electrodes to the gate electrode should be first attained in order to provide printed TFT-based devices that function on par with Si-based devices.

Limits of overlay printing registration accuracy (OPRA) in printed TFTs: Fully printed TFTs with a short channel length ($< 10\ \mu$m) and gate width ($< 30\ \mu$m) are not practically achievable yet, due to the limits associated with OPRA when using currently available printing systems. OPRA will be the most important criteria in determining the characteristics of fully printed TFTs since gate electrodes and drain-source electrodes should be well aligned to insure proper device operation and mitigate device variation. Therefore, fully printed, TFT-based products should be well matched to the limits of OPRA in a printing system. In addition to the printing system's mechanical capabilities, the interdependencies with the ink and the substrate must also be considered in order to define the limits of OPRA. Attainable printed TFT-based products based on currently achievable OPRA are shown in Fig. 3. Printing systems can be largely divided into either roll-to-roll (R2R) or sheet-to-sheet (S2S) printing systems based on the substrate feeding method. The current limits of OPRA ($\pm 20\ \mu$m for R2R and $\pm 10\ \mu$m for S2S) will be improved to $\pm 5\ \mu$m for R2R and $\pm 1\ \mu$m for S2S by employing a laser based registration control system used in photolithographic processes by the semiconductor

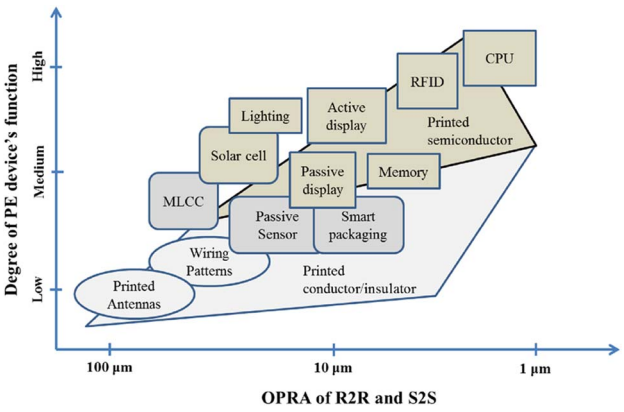

Fig. 3. *Schematic description of expected IT products based on fully printed TFTs, as a function of the Overlay Printing Registration Accuracy (OPRA) limitations for a roll-to-roll (R2R) and sheet-to-sheet (S2S) printing systems.*

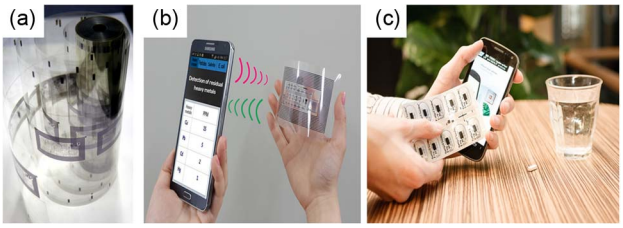

Fig. 4. ***Concept images of (a) R2R printed TFT-based RF tags, (b) RF e-sensor tag, and (c) smart packaging (Imec news, Eindhoven-July 17, 2012).***

industry. Based on those OPRA, R2R or S2S printing technology [9] could practically and reliably manufacture the integrated TFT circuits either on flexible sheets or on rolls with electrical characteristics that could compare to amorphous Si-based TFTs in 5 years. The advent of printed electronics would then create new IT markets *via* low-cost RF tags, RF-sensor tags, and smart packaging (Fig. 4).

OPRA and device physics understanding are needed for printed TFTs: Although, current R2R and S2S printing systems can provide the OPRA to integrate TFTs of a reasonable size and a medium level of integration, unfortunately, well-established printing systems that would use finely tuned materials for TFT fabrication cannot be used because the fundamental physics of TFTs is dominated by surface effects and interfacial phenomena, which differs substantially from traditional media printing. In media printing, all printing systems, including servomechanisms, printers, inks and printed products, have been fully established based on human perceptive requirements and can tolerate 100 μm misalignments in such a way that those printing systems are sufficient for the attainment of high visual quality printed color images [10]. Printed TFTs, however, are quite different and will be significantly affected by defects of even a few nanometers at interfaces between printed layers, as these usually lead to device failure. Furthermore, even with no physical defects and the same physical dimensions in printed layers, the electrical output currents from printed TFTs will vary among printed devices because V_{th} variation arises due to variable capacitance and trapped charges [11]. The issues originate from fluctuations in gate lengths, gate widths, gate dielectric layer thicknesses, surface roughness and the effect of ink additives that may act as dopants in semiconducting ink and fixed or mobile ions in dielectric inks [12], [13]. The variability that is introduced by each layer will determine the V_{th} variation, which limits the number of integrated TFTs in a logic circuit [14], [15].

Differences between partially printed and printed TFTs: A number of flexible TFT-based devices consisting of at least one printed layer have been announced as printable devices, and referred to as partially printed TFT (*pr*-TFT) based devices, in order to emphasize the potential of printed electronics and avoid problems caused by V_{th} variation [16]–[20]. However, the highlighted performances of *pr*-TFT based devices fabricated using at least one layer of vapor deposition or spin-coating to minimize the V_{th} variations cannot be replicated in a fully printed process. Because the substitution of vapor-deposited or spin-coated layers cannot be simply realized through a printing method, the attainment of comparable electronic properties and reliability using a full-printing process is highly questionable. This is a major reason why the successful launch of printed TFT-based electronics in the IT marketplace has been thwarted despite many high-profile demonstrations showing versions of flexible, roll-able and even stretchable *pr*-TFT-based devices over the past 10 years. The key issues in replicating *pr*-TFT-based devices with fully printed TFT-based devices are related to control the V_{th} variation through understanding the unique characteristics of the inks and their transfer mechanisms. The V_{th} of printed TFTs fluctuates according to several structural factors such as edge waviness, feature width, quality of the interface between layers and surface roughness, all of which are very sensitive to the printing environment and ink rheology. A more problematic issue is the difficulty in elucidating nonstructural factors [21]. In particular, the trapped charges, the DOS, the band gap, and the work function of conducting, semiconducting and dielectric inks are all very sensitive and vary according to the selection of solvents and binders used to control rheological properties during ink formulations [22], [23]. Therefore, minimizing the V_{th} variation in fully printed TFTs will be prohibitively difficult without an understanding of the printing process in conjunction with the phenomena of charge (electron and hole) transport that will vary depending on ink formulation, printing mechanics, the rheology of inks, and the resulting interfaces [24]–[26]. Only a few studies have focused on explaining the variations in charge transport properties for *pr*-TFTs [27], [28]. In other words, the phenomenon of charge transport in fully printed TFTs are not fully understood or even simulated with printing systems in mind.

Scope of this article: The present review focuses on the crucial factors that have direct impact on V_{th} variation in fully printed TFTs. By considering the effect of trapped charges and capacitance variation in conjunction with the mechanics of the printing process and ink rheology we will clearly show the relationship between the V_{th} variation in printed TFTs and the mechanics of the printing process. After addressing the V_{th} variation, we will present the fabrication of prototypes that utilize a minimum number of fully printed TFTs in order to construct functional circuits that not only overcome the critical V_{th} variation that deteriorate the performance of printed electronics but provide a viable path to commercialization. The prototypes are fully printed RF sensor-labels [29] and RF *e*-sensor (cyclic voltammetry) tags [30]. These prototypes have been fully R2R or S2S gravure printed and can be considered as a

platform that can be expanded into a variety of disposable and ubiquitous electronic devices by adding a logic controller, an ADC and a shift register as the range of the V_{th} variation is narrowed. The prototypes of fully printed RF sensor labels and tags are reviewed and discussed in the following order:

1) Acceptable V_{th} variation ranges for fully printed TFTs in RF sensor devices.
2) Integration of printed TFTs.
3) Fully printed passive RF *e*-sensor tags with a low integration of printed TFTs.

II. ACCEPTABLE VARIATION RANGES FOR THRESHOLD VOLTAGE OF TFTs FOR PROPER OPERATION OF AN RF SENSOR DEVICE

Although we do not clearly understand the relationship between electrical properties of fully printed TFTs, electronic inks and ink transfer mechanisms, printed TFT-based devices provide a compelling opportunity compared to *pr*-TFT and Si based devices if they could be manufactured using high throughput processes on plastic or on paper foils. To achieve this, a reasonable number of TFT with a narrow V_{th} variation must be integrated on a flexible substrate using a high throughput printing process, such as R2R gravure. What must be overcome is the process-induced variation of V_{th}. This becomes critical when integrating TFTs to fabricate functional circuits. Ideally, each device would have virtually identical V_{th} so when switching them on and off all TFTs would do so simultaneously and consequently match to deliver digital signals to neighbor devices with readable noise margin and without significant signal delay. Therefore, as the variability of V_{th} increases, an output signal decreases, resulting in a circuit failure.

With this objective in mind we then determined the viable operating space for our process. The range of variation from the target V_{th} of TFTs directly limits the degree of integration and functionality of the printed devices because the output currents and voltages from each TFT rely on the V_{th} variation, which is a barometer of the capacitance and trapped charges in TFTs [31]. As shown in equation: $\Delta V_{th}(t) = eN_{tr}(t)/C_o$), the variation in the V_{th} is closely related to both the change in capacitance (C_o) which is related to the printed physical dimensions, such as the thickness, surface roughness, and edge waviness of printed patterns and the trapped charge density (N_{tr}) [21], [32]. Therefore, trap charges in the semiconducting layer and fixed or mobile charge in the dielectric layer due to the intrinsic impurities of the inks or environmental influences (oxygen, water and light) must be carefully controlled. Based on our previous studies and results reported by others, we determined that we could mass produce fully printed RF sensor devices depending on the number of integrated TFTs with < 30% V_{th} variation (Table 1) [29], [30], [33] because the V_{th} variation more than 30% would lead to device failure or very low gain of the logic circuit. Please note, the envisioned devices and data shown in Table 1 are extracted only from fully printed TFT-based devices on plastic foils using no vapor deposition, photolithography, laser ablation or spin coating.

The proposed R2R gravure printing scheme (Fig. 5) described here can be used to manufacture passive RF sensor devices with an integration of less than 100 TFTs because it can achieve the desired 30% V_{th} variation at the target V_{th} (as described below) on 150 m of poly(ethylene terephthalate) (PET) roll with 250 mm web width [34]. First, the antenna, wires and electrodes are printed. The dielectric layers are printed in the second printing unit. The active layers for the diodes are printed in the third unit, and active layers for the TFTs are printed in the fourth unit. All

Table 1 Proposed Specifications for Mass-Production of Fully Printed RF Sensor Devices With the Required Integration Number of Printed TFTs

Fully printed target devices	Passive RF label sensor label	Passive RF *e*-sensor tag	NFC Smart tag*
# of integrated TFTs	0	20~100	100~5000
Acceptable variation range (%) at the target V_{th}	No need	± 30	± 30 ~ ± 10**
Charge-carrier mobility (cm^2/Vs)	No need	0.01-0.1	0.1 – 1.0
Operation voltage (V)	~ 20	1.5~20	< 2
Operation speed (Hz)	No need	1 -10	~ 100 k
Remarks	Need diodes for rectifier	Indicate Yes or NO	Interlock with smartphones

*A simplified transponder can be constructed using a minimum number of printed TFTs. **± 10 % was estimated based on Monte Carlo simulations using a full adder circuit with 55 TFTs.

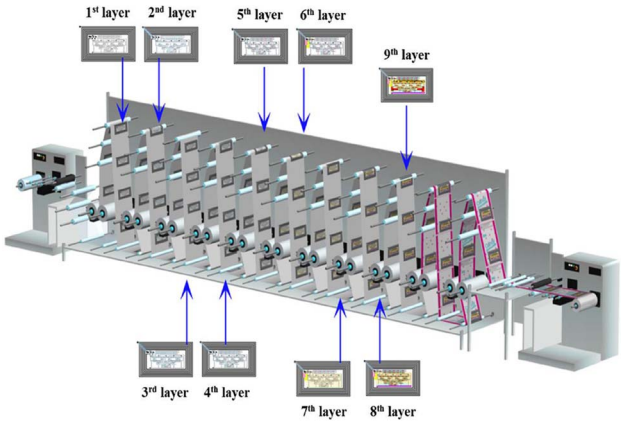

Fig. 5. *Descriptive scheme for R2R gravure printing system used to print RF sensor tags and smart packaging on a single line.*

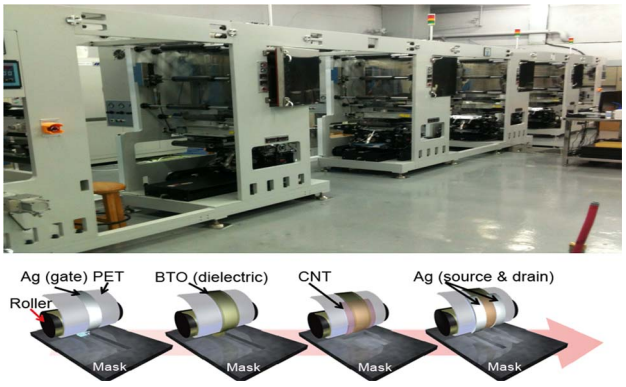

Fig. 6. *Real image of a S2S gravure printer that houses 4 printing units with a registration accuracy of ±10 μm and a step-by-step printing scheme for the continuous printing of TFTs.*

top electrodes for capacitors and drain-source electrodes are printed in the fifth printing unit. The top electrodes of the diodes are printed using low work function metal ink in the sixth printing unit. The insulating layers needed to prevent shorts caused by crossing wires used to contact diodes and antennas are printed in the seventh printing unit, and the final wires used to complete the circuit are printed in the eighth unit. Finally, the fully gravure printed RF sensor tags are laminated at the ninth printing unit. After the laminating step, packaging is continuously printed as an inline printing process. This R2R gravure process seamlessly integrates passive RF sensor tags with traditional printing to enable smart packaging with less than 100 printed TFTs through high throughput manufacturing.

III. INTEGRATION OF PRINTED TFTs

While many *pr*-TFT-based functional circuits have been reported, only a few fully printed TFT-based functional circuits have been demonstrated [29], [30], [33]. The major reason for this lack of fully printed functional devices originates from a variation in threshold voltage (V_{th}) that is related to the variability in the printed layers of TFTs in the circuit [35], [36].

To attain an acceptable variation in the V_{th} of fully printed TFTs, controlling the registration accuracy of printed drain—source electrodes to the gate electrode was the first priority to remove obvious variable factor in the static and dynamic characteristics of TFT [37]. Therefore, the OPRA should be in the range of ±10% to eliminate the obvious contribution to the fluctuation of TFT [38]. To attain ±10% registration accuracy from scalable printing methods, the use of sheet-to-sheet (S2S) gravure (Fig. 6) is the most appropriate. It will provide ±10 μm registration accuracy and can be easily transferred to the R2R gravure system with ±20 μm registration accuracy for mass production [39]. In the present study, to compensate for 10% misalignment, a channel length ranging between 100 and 150 μm was deemed appropriate for a 250 μm gate width [40]. As shown in Fig. 7, the variations in the V_{th} of 30 fully printed TFTs with channel lengths of 150 μm maintained within a 30% range using the S2S gravure printing system [41].

After removing the influence of misalignment on the V_{th} variation by selecting the optimized channel length for a given S2S gravure printing system, we addressed the remaining factors that contribute to the V_{th} variation such as ink rheology, because the ink transfer rate is closely related to the viscosity of the ink [42]. Furthermore, the rheological behavior of electronic inks is very sensitive to even small variations in temperature and humidity while the controlling systems of printers, such as tension and nip pressure control, are maintained at constant levels. However, our results showed that the rough surface morphology and edge waviness (5 ∼ 8 μm) of printed gate electrodes and wires did not seriously affect the V_{th} since the attained roughness was mitigated by the over-printing dielectric layers, and the channel length used (100 ∼ 200 μm) is

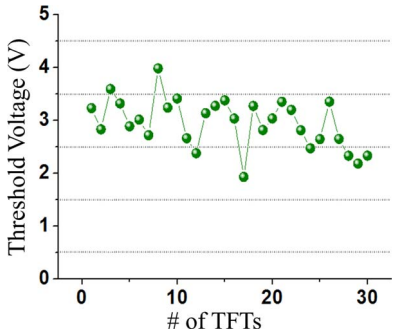

Fig. 7. *Variation of the V_{th} for 30 fully S2S gravure-printed carbon nanotube based TFTs with channel lengths of 150 μm.*

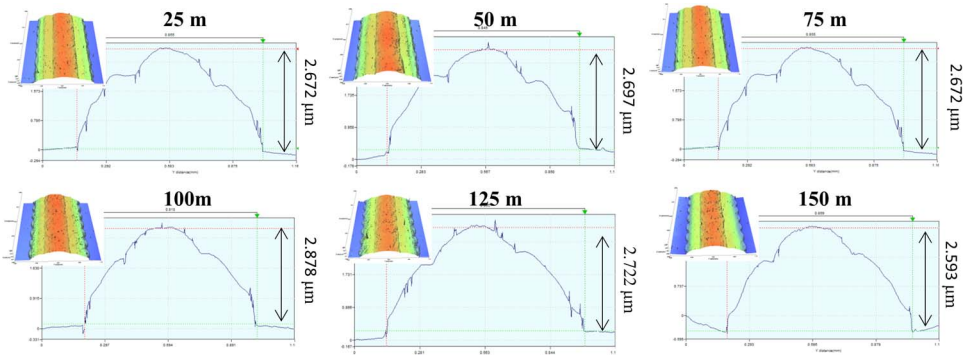

Fig. 8. ***Thickness variations in R2R gravure printed dielectric layers along 150 m of a PET roll.***

compensates for the edge waviness of the printed gate electrodes.

Unlike conductive inks used for gate electrodes, the rheology of dielectric inks is the most critical factor in printed TFTs since the density of mobile and fixed charges originate from heterogeneous dielectric layers [43], and by the interface with other layers e.g., semiconducting layer [44]. Furthermore, the morphology of printed dielectric layers will affect the formation of irregular semiconducting layers because wetting by the semiconducting ink varies according to the surface roughness [45]. This means that dielectric ink with an ion-free or a constant-ion density should always be used, and the rheology of the dielectric ink should be well controlled to insure consistency in the ink transfer rate and the surface morphology. Consistency in both the dielectric ink transfer rate as well as in the surface morphology of printed dielectric layers are pivotal factors in providing consistent capacitance through thick printed dielectric layers. Fig. 8 shows the thickness variation in printed dielectric layers through R2R gravure printing on 150 m × 0.25 m of PET roll with a humidity variation of ±10% and a temperature variation of ±10% [34]. However, when the viscosity of the dielectric ink is changed by as much as 10%, the morphology of printed dielectric layers will change dramatically even under constant gravure printing conditions. As shown in Fig. 9, the surface morphologies of printed dielectric layers were changed from an ideal parabolic to a sharp-edged one (coffee stain) under the same gravure printing conditions when using inks with viscosities of 64 and 52 cP, respectively. Those small microscopic changes in the morphology of the printed dielectric layers led to a large difference in the capacitance ($\sim$7 nF/cm^2) and in the irregularity of semiconducting layers. Those differences resulted in markedly different V_{th} values for printed TFTs even when using the same semiconducting inks.

Printed semiconducting layers are very sensitive to surface morphology, and surface energy also influences

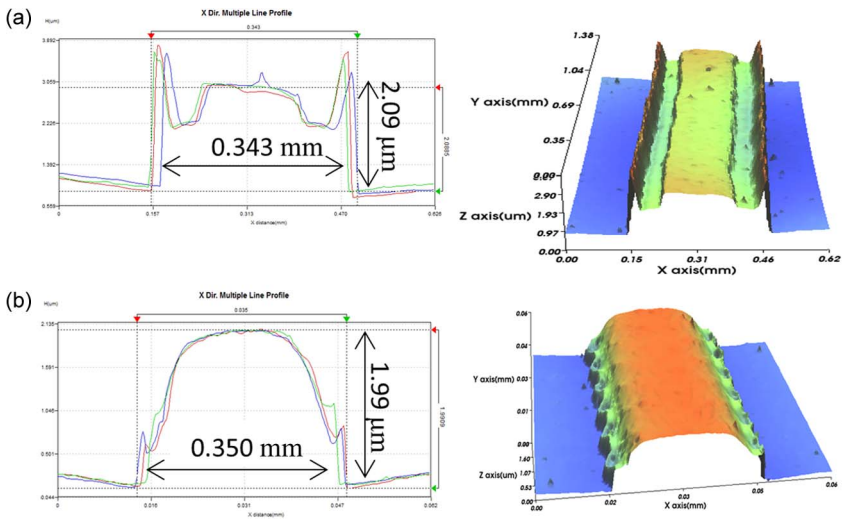

Fig. 9. ***Cross-sectional images of printed dielectric layers using (a) 64 cP and (b) 52 cP inks under constant gravure printing conditions.***

the formation of semiconductor domain boundaries [46]. Microscopic changes in the morphology of printed dielectric layers result in completely different TFTs even when using the same semiconducting ink, because surface energy variation in printed dielectric layers changes the ordered crystalline domains structures of printed semiconductors and consequently generates fluctuations in the V_{th} for each printed TFT [47]. These results showed that even a small local change in the surface energy or a microscopic change in the surface morphology of the printed dielectric layers will generate variations in the V_{th} of printed TFTs.

The last issue we will consider that causes fluctuations in the V_{th} of fully printed TFTs is uneven contact resistance between printed drain-source electrodes and semiconducting layers. Tuning the work function of silver ink to a given organic semiconductor is critical in providing reliable printed TFTs. Thus far, silver nanoparticle-based inks have been the only practical option to print drain-source electrodes with sufficient conductivity and appropriate work function level for printed semiconductor based TFTs. Unfortunately, the work function of printed silver is very sensitive to ink formulation and printing conditions. In fact, the work function of silver nanoparticle-based ink can be altered by up to ± 0.3 eV by simply changing the binder molecules during the formulation of the ink, because the binder molecules will modify the dipole moment of silver nanoparticles and consequently change the work function of printed silver electrodes [48]. The sensitivity of silver nanoparticles to binder molecules often causes V_{th} variations in printed TFTs, because the amount of binder on a silver nanoparticle varies depending on the printing temperature and the dilution of the silver ink. Fig. 10 shows a typical change in contact resistance for printed TFTs when simply diluting the silver inks with ethylene glycol or diethylene glycol. Work-function matching must first be addressed by the silver ink formulation in order to obtain near-ohmic contacts in printed TFTs.

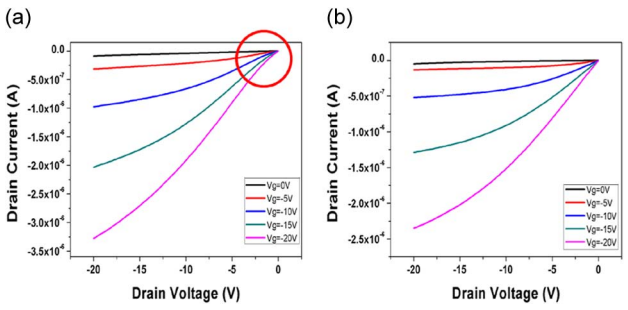

Fig. 10. *The output characteristics of printed TFTs using silver nanoparticle based ink diluted with (a) ethylene glycol and (b) diethylene glycol to print drain-source electrodes. The red circle indicates contact resistance generated due to the mismatch of source-drain contact.*

Fully printed organic semiconductor-based TFTs (*O*-TFT) for logic devices with an integration level of more than 30 transistors have not been demonstrated using a scalable printing method due to impractical channel length ($< 30\ \mu$m) and power consumption in the resulting devices. In other words, *O*-TFT do not perform up to expectations when using a scalable printing process because the high surface roughness of the dielectric layers combined with the large channel lengths typically achieved with scalable fabrication methods ($> 150\ \mu$m) lead to high V_{th} variation and prohibitive power consumption. Hence, we focused our efforts on carbon nanotube (*Cn*)-based TFTs given that fully printed *Cn*-TFT-based logic gates operate at reasonable power levels (20 V) [49]–[51]. Based on fully gravure-printed TFTs with a network structure of single-walled carbon nanotubes as a semiconducting layer, the V_{th} variation can be controlled within $\pm 30\%$ (Fig. 7). This enables the integration of 100 *Cn*-TFTs using R2R gravure (Fig. 5) for logic gate-based functional devices that can be operated at 20 V DC, based on *P*SPICE simulation (Fig. 11). For printed *Cn*-TFTs, an epoxy based SiO_2 composite ink with a viscosity of 400 cp was used to print a passivation layer with a thickness of 4 μm and width of 500 μm on top of the printed *Cn*-TFTs. After the passivation, the printed *Cn*-TFTs were dried at 100 °C in an oven for 10 min. Based on this passivation process, we were able to minimize the change in V_{th} even when operating the *Cn*-TFT-based inverter under conditions of high (95%) humidity.

Although the shift range of the V_{th} could theoretically be controlled to some degree in order to integrate approximately 400 printed *Cn*-TFTs, those printed devices cannot wirelessly interlock with the NFC function of a smartphone nor can they utilize energy-harvesting schemes because DC 20 V is required for the proper operation of printed *Cn*-TFT-based devices. To interconnect with the smartphone *via* NFC, the printed devices should operate at < DC 2 V because wirelessly transmitted power from the smartphone *via* 13.56 MHz is picked up by antenna and converted into usually less than DC 2 V depending on the antenna design, the impedance, etc. Therefore, lowering the operation voltage to less than DC 2 V for printed devices is the next important issue to be addressed. Although electrolyte gels and self-assembled monolayers (SAM) have been successfully utilized as dielectric layers to maximize gate capacitance for the reduction of operation power to a level of DC 2 V [52], [53], these processes are not yet scalable. Alternatively, fully gravure-printed CMOS-type *Cn*-TFT-based inverters [see Fig. 12(a) and (b)] can operate at a power level of DC 5 V. A *Cn*-TFT-based all S2S gravure-printed CMOS-type ring oscillator has been developed by employing thermally curable epoxy-imine-based *n*-doping ink. Gravure printing this ink provides an easy path to encapsulated *n*-channel *Cn*-TFTs by curing immediately after printing. Furthermore, by simply enriching a semiconducting carbon nanotube ink to 95%

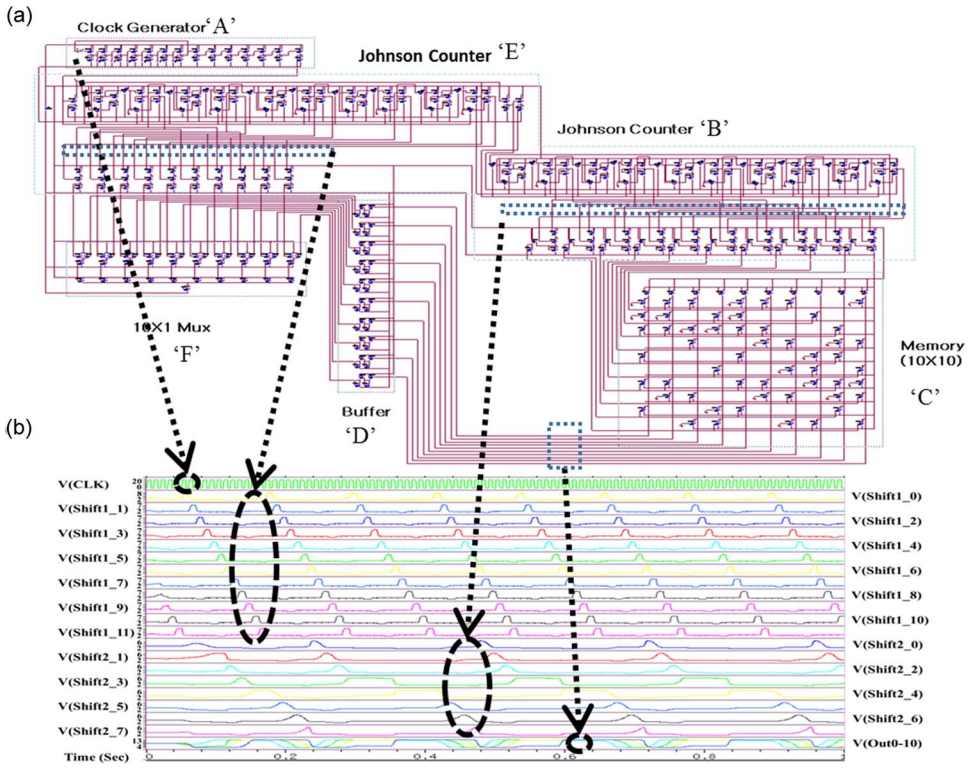

Fig. 11. ***A circuit design and its simulation output for about 400 transistors using parameters extracted from fully printed TFTs with a network of single-walled carbon nanotubes as the semiconducting layer. This simulation indirectly proves that a 30% V_{th} variation range is feasible for a fully printed integrated circuit with 400 TFTs even when containing read-only memory units.***

purity, a fully gravure-printed ring oscillator that consisted of 5 stages of a CMOS-type *Cn*-TFT-based ring oscillator can be operated at DC 2 V, as shown in Fig. 12(c).

Although current gravure printing systems that utilize conducting, semiconducting, and dielectric inks can produce fully printed *Cn*-TFTs with a V_{th} variation range of $\pm$30% and good environmental stability, the available integration density is limited to $<$ 100 TFTs because the device yield is currently too low ($<$ 70%). In addition to the issues previously discussed regarding the V_{th} variation, the PET substrate is deformed microscopically while undergoing through a series of heating and cooling cycles under constant web tension, also impacting the device yield. Therefore, competitive products for fully printed disposable devices including integrated wireless sensor devices with a minimum number of printed *Cn*-TFTs will appeal to niche markets that Si-based devices cannot satisfy. The remainder of this paper introduces fully printed RF sensor devices with 26 printed *Cn*-TFTs using only a scalable gravure printing method.

IV. FULLY PRINTED RF *e*-SENSOR TAGS WITH LOW INTEGRATION OF PRINTED TFTs

Disposable RF sensor-labels can be fully fabricated by printing 13.56 MHz antenna, diodes, capacitors, sensors, and simple signage without integrating any printed *Cn*-TFTs (Fig. 13) [29]. However, they are limited to only simple applications because these partially printed sensors in the label are all simple passive devices that cannot be used to analyze specimens. However, for effective sensing of our surroundings and product quality monitoring, a sensor should be able to analyze multi-specimens with some degree of selectivity. Therefore, for the universal application of RF-sensor labels, a printed sensor should be constructed based on the most common phenomena of a given material such as electron transfer [54], mass change [55], refractive index alternation [56], etc., so that the RF-sensor label can detect a wide range of specimens with a single sensor.

Potentiometric, amperometric, and conductometric based electrochemical sensors offer high analytical performance for a wide range of gas and liquid analytes [54]. In particular, portable electrochemical transducers, which convert chemical information into electrical signals, have long been utilized as alternatives to expensive and bulky analytical instruments.

Although these sensors (potentiometric and amperometric) have benefits that include cost-effectiveness and convenience in usage, currently available electrochemical sensors are burdened by the following deficiencies:

1) Reliability: The calibration step can be a possible source of error. Furthermore, the matrix of analyte

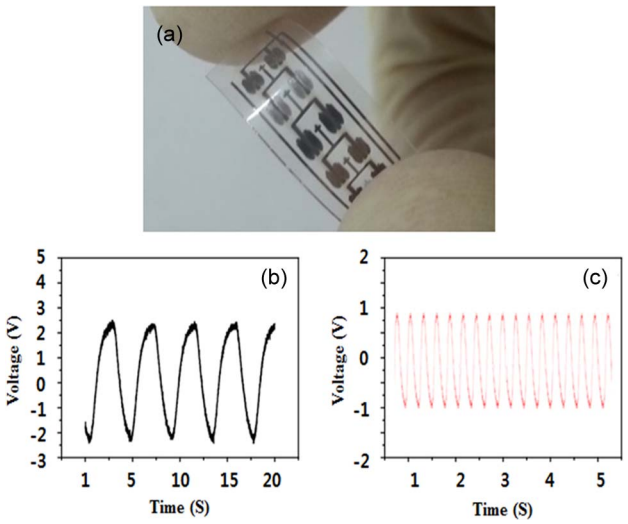

Fig. 12. *(a) The image of a fully gravure-printed CMOS-type inverter based ring oscillator, (b) generated output signal by DC 5 V, and (c) DC 2 V. The output frequency (c) of a CMOS-type based ring oscillator is higher than that of (b) even under lower DC voltage because semiconducting carbon nanotube enriched (99%) aqueous ink without a polymer binder was used to print the ring oscillator (c) while a mixture of metallic and semiconducting carbon nanotube ink with a polymer binder was used for the ring oscillator (b).*

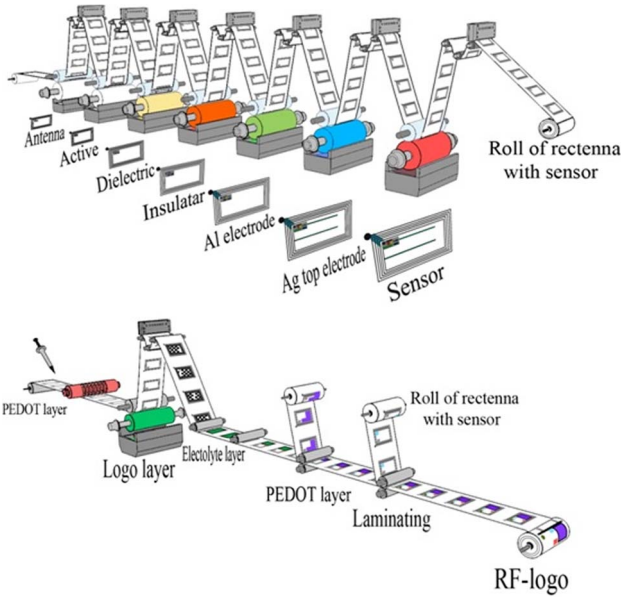

Fig. 13. *A descriptive scheme for a R2R manufacturing process for RF labels and RF-sensor labels [29]. In the first R2R gravure printing unit, silver nanoparticle based ink was used to print antennas and bottom electrodes for diodes and capacitors. In the second printing unit, ZnO based ink was selectively printed onto the bottom electrodes of a diode, and then, at the third printing unit, dielectric layers were printed on the bottom electrodes of the capacitors. At the fourth printing unit, an insulating layer was printed using epoxy based ink to print insulating layers on a silver connection between the diodes and the antennas. At the fifth printing unit, aluminum paste was used to print the top electrode for the diodes, and then consecutively print a silver connection and top electrodes for the capacitors in the sixth printing unit. In the final printing unit, a humidity sensor was printed using conductive polymer based ink. To complete the fabrication of the RF QR sensor Tags, the printed rectifier roll with a sensor was laminated onto PEDOT-based electrochromic signage, which was also prepared using a R2R coating process.*

solutions (e.g., a glucose sensor that contains a different blood matrix) can affect the magnitude of the electric signals, which renders the obtained data inaccurate.

2) Versatility: Since the sensor should respond only to a target analyte, the indicator electrodes must be judiciously prepared to be specific to the analyte. This means that both potentiometric and amperometric sensors have inherent limitations in multipurpose use.

In this regard, a possible solution could be the use of voltammetric sensors that can simultaneously scan the potential applied on a working electrode while measuring the potential-dependent current. The operating principle of a typical cyclic voltammetry (CV) experiment [57] is shown in Fig. 14.

Since the half-wave potential ($E_{1/2} = (E_{pa} + E_{pc})/2$) is sensitive to the identity of analytes, and the peak current (i_{pa} and i_{pc}) is proportional to the concentration of analytes in CV, voltammetric sensors can be applied to the detection of most chemical species with moderate standard reduction potentials. Based on this redox reaction potential, the analytes can be detected and even selectively differentiated by the level of picomoles. In this way, not only chemicals and metals, but also a variety of pathogenic bacteria [58], viruses [59], proteins [60] and DNA [61] can be detected to the level of ppm in an *in vitro* system. Therefore, if a CV could be simplified and integrated onto a flexible and disposable substrate at extremely low manufacturing cost, this would create a new universal RF-sensor label, which could be referred to as a "RF *e*-sensor tag" system in order to differentiate it from simple "RF-sensor label" systems with no printed TFTs.

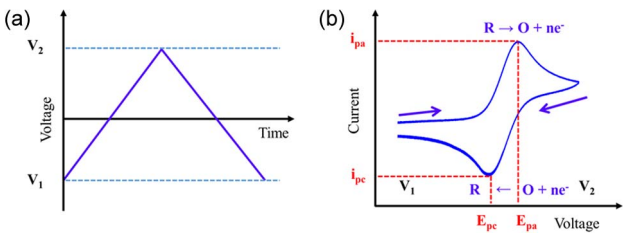

Fig. 14. *(a) A triangular wave (< 1 Hz) to scan (b) an electrochemical cell and a typical cyclic voltammogram showing reversible behaviors. Epa: anodic peak potential; Epc: cathodic peak potential; i_{pa}: anodic peak current; i_{pc}: cathodic peak current; and arrows: scan direction.*

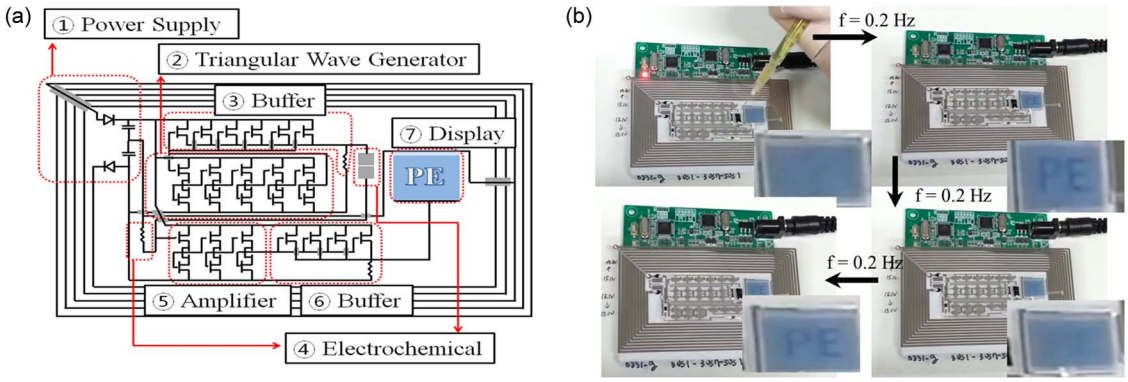

Fig. 15. ***Schematic circuit layout (a) and real operation images of a fully gravure-printed passive RF e-sensor tag (b). Figure (b) shows the operation of RF e-sensor tag where "PE" signage blinks on and off with a low frequency only at a certain level of analyte concentration in the specimen while no signage is displayed at lower analyte concentration in the specimen [62].***

To manufacture a CV based sensor at extremely low cost, the basic layout for a single-use, disposable CV sensor, called the "passive RF *e*-sensor tag" has been developed and appears in Fig. 15(a) [62].

The passive RF *e*-sensor tag shown in Fig. 15(a) can be fully printed using scalable R2R and S2S printing methods on plastic foils because only 26 integrated *Cn*-TFTs would be required to support the function of a CV. In fact, based on the *P*SPICE simulation of fully printed *Cn*-TFTs on plastic foil, about 30% threshold voltage (V_{th}) variation from 26 TFTs is acceptable for the proper operation of the designed RF *e*-senor tag circuit.

To realize a RF *e*-sensor tag using scalable printing methods, R2R gravure was first employed to print a rectenna [① in Fig. 15(a)], which consisted of a divided antenna, 2 diodes and 2 capacitors to provide positive and negative DC voltage to the printed ring oscillator. By using the printed rectenna as a substrate, a 5-stage ring oscillator [② in Fig. 15(a)] consisting of 10 *Cn*-TFTs was printed using S2S gravure and was used as a pseudo triangle wave generator to scan printed electrochemical cells [④ in Fig. 15(a)]. Finally, 3 series of inverters consisting of 6 *Cn*-TFTs were also printed using S2S gravure and were used as amplifiers [⑤ in Fig. 15(a)] to enhance the output currents after scanning the printed electrochemical cell that consisted of printed carbon and silver electrodes. Between those printed electrodes, a $LiCF_3SO_3$-based gel type of electrolyte was printed to provide an environment that could enable an electrochemical redox reaction after the application of one drop of aqueous or organic solution.

Although the operation power can be wirelessly transmitted from the 13.56 MHz RF reader, the attained output currents after scanning the electrochemical cell in the tag cannot be sent back wirelessly to the 13.56 MHz RF reader to analyze and share the data *via* the Internet because the data processing speed (< 100 Hz) from the fully printed RF *e*-sensor tag cannot meet the required speed (> 100 kHz) from either a smartphone or a RF reader. This is why the modulation TFT in Fig. 15(a) in the RF *e*-sensor tag is unnecessary given the current status. However, printed signage [⑦ in Fig. 15(a)] has been easily integrated in order to display the presence of an analyte in the solution using output currents from the electrochemical cell.

In the proximity of a 13.56 MHz RF reader (3A logics RSK 100), the fully printed RF *e*-sensor tag will couple 13.56 MHz of AC and then convert it to polarized DC [① in Fig. 15(a)]. The polarized DC will run the printed ring oscillator to generate the pseudo triangle wave at a low frequency (< 1 Hz) [② in Fig. 15(a)]. The triangle wave will scan the printed electrochemical cell to perform a redox reaction [④ in Fig. 15(a)]. The output currents after the redox reaction triggered by a drop of specimen will be amplified by passage through the printed amplifier [⑤ in Fig. 15(a)], which will cause the signage [⑦ in Fig. 15(a)] to blink with a given frequency produced by the printed ring oscillator. However, if no analyte is present in the specimen, the signage will not be activated. The operation sequence is shown in Fig. 15(b) using a captured still-cut image. This printed RF *e*-sensor tag could be used as a platform for a universal sensor to detect a variety of analytes that includes air-borne and water-borne contaminants.

Although the ultimate goal of this printed RF *e*-senor tag is to wirelessly interlock with a NFC-function-housed smartphone, it is not compatible with the smartphone yet because of high operation voltage (∼DC 20 V). However, the fully printed RF *e*-sensor tag will soon be expected to operate at DC 1.5 V by employing CMOS-type printed *Cn*-TFTs with enriched semiconducting single-walled carbon nanotube ink [63].

Finally, a future goal is a printed RF *e*-sensor tag that can be used to enable the Internet of Things (IoT) with a cost that will range from $0.05 to $1 depending on the required function [64]. The evolution of printed RF *e*-sensor tags that can reach the level of IoT is also called an "NFC smart tag" where sensor arrays, display and general

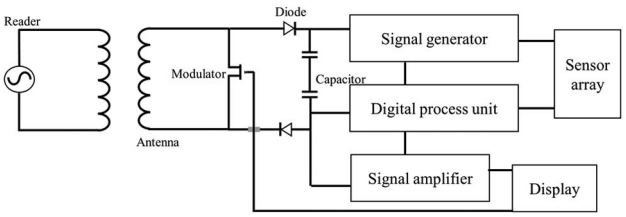

Fig. 16. ***Layout of the fully printed NFC smart tag.***

processors are all printed as shown in Fig. 16. Although such an IoT-compatible, fully printed, smart tag is beyond the current level of printed TFT-based wireless devices, a NFC smart tag (Table 1) could be fully printed when the OPRA can be controlled to a level of ± 1 μm by using commercially available electronic inks. Of course, plastic and paper substrates must also be further developed to the level of glass substrates in order to achieve angstrom level surface smoothness and to prevent the permeation of water and oxygen through the substrate.

V. CONCLUSION

After reviewing fully printed and partially printed TFTs, crucial performance factors in partially printed TFTs that cannot be reproduced by current printing processes were extracted and analyzed to develop a practical strategy to successfully manufacture fully printed TFT based flexible devices. The extracted factors are all directly related to the V_{th} variation in fully printed TFT based flexible devices that result from variations in trapped charges, contact resistance and capacitance between each of the printed layers and on the mechanics of the printing process as well as on the ink rheology. A hybrid printing process that includes vacuum deposition steps to fabricate TFT based flexible devices may have better control over some of these factors but cannot be directly transferred to a scalable printing process. With further development, we believe that a fully printed process will surpass a hybrid printing process in manufacturing electronic devices if the driver is high volume and low cost. In this respect, we have shown that a R2R printed RF *e*-sensor label can be realized by integrating fully printed TFTs. As an example of what can be practically manufactured, we described herein a fully gravure printed RF *e*-senor label needing only 26 printed TFTs, capable of performing cyclic voltammetry (CV) for analyte detection. The RF *e*-senor approach will be further enhanced by wireless communication with a smartphone and used as a disposable test kit in both environmental and health diagnosis. Furthermore, this approach will become more sophisticated by increasing the number of integrated TFTs as the servomechanisms of printers improves the overlay printing registration accuracy to ± 1 μm (with associated reduction in V_{th} variation) and device yield. Also, new device physics concepts for printed TFTs will be established to help explain the relationship between the electrical characteristics of printed devices and the rheology of the inks and mechanics of transfer during printing. ■

Acknowledgment

The authors acknowledge the valuable advice and comments from Dr. P. R. L. Malenfant (National Research Council of Canada).

REFERENCES

[1] K. Fukuda, Y. Takeda, M. Mizukami, and S. Tokito, "Fully solution-processed flexible organic thin film transistor arrays with high mobility and exceptional uniformity," *Sci. Rep.*, vol. 4, no. 3947, 2014.

[2] T. Ng *et al.*, "Scalable printed electronics: An organic decoder addressing ferroelectric non-volatile memory," *Sci. Rep.*, vol. 2, no. 585, 2012.

[3] J. Chang, X. Zhang, T. Ge, and J. Zhou, "Fully printed electronics on flexible substrates: High gain amplifiers and DCA," *Org. Electron.*, vol. 15, pp. 701–710, 2014.

[4] D. Schwartz and T. Ng, "Comparison of static and dynamic printed organic shift registers," *IEEE Electron Device Lett.*, vol. 34, no. 2, pp. 271–273, 2013.

[5] M. Jung *et al.*, "All-printed and roll-to-roll-partially printed 13.56-MHz-operated 1-bit RF tag on plastic foils," *IEEE Trans. Electron Devices*, vol. 57, no. 3, pp. 571–580, 2010.

[6] Y. Yuan *et al.*, "Ultra-high mobility transparent organic thin film transistors grown by an off-centre spin-coating method," *Nat. Commun.*, vol. 5, no. 3005, 2014.

[7] M. Kitamura and Y. Arakawa, "High current-gain cutoff frequencies above 10 MHz in n-channel C_{60} and p-channel pentacene thin-film transistors," *Jpn. J. Appl. Phys.*, vol. 50, p. 01BC01, 2011.

[8] F. Ante *et al.*, "Contact resistance and megahertz operation of aggressively scaled organic transistors," *Small*, vol. 8, pp. 73–79, 2012.

[9] J. Noh *et al.*, "Scalability of roll-to-roll gravure-printed electrodes on plastic foils," *IEEE Trans. Electron. Packag. Manuf.*, vol. 33, pp. 275–283, 2010.

[10] W. J. Donnelly, F. Romero-Borja, and A. Roorda, "Optimal pupil size for axial resolution in the human eye," *Invest. Ophthalmol. Vis. Sci.*, vol. 42, p. 161, 2001.

[11] T. Ha, D. Kiriya, K. Chen, and A. Javey, "Highly stable hysteresis-free carbon nanotube thin-film transistors by fluorocarbon polymer encapsulation," *ACS Mater. Interfaces*, vol. 6, pp. 8441–8446, 2014.

[12] W. Kalb and B. Batlogg, "Calculating the trap density of states in organic-effect transistors from experiment: A comparison of different methods," *Phys. Rev. B*, vol. 81, p. 035327, 2010.

[13] W. Kalb, S. Haas, C. Krellner, T. Mathis, and B. Batlogg, "Trap density of states in small-molecule organic semiconductors: A quantitative comparison of thin-film transistors with single crystals," *Phys. Rev. B*, vol. 81, p. 155315, 2010.

[14] S. M. Kang and Y. Leblebici, *CMOS Digital Integrated Circuits*, 3rd ed. New York, NY, USA: McGraw-Hill, 2003.

[15] D. A. Neaman, *Electronic Circuit Analysis and Design*, 2nd ed. New York, NY, USA: McGraw-Hill, 2001.

[16] B. Crone *et al.*, "Large-scale complementary integrated circuits based on organic transistors," *Nature*, vol. 403, pp. 521–523, 2000.

[17] G. H. Gelinck *et al.*, "Flexible active matrix displays and shift registers based on solution-processed organic transistors," *Nature Mater.*, vol. 3, p. 106, 2004.

[18] K. S. Soeren *et al.*, *Solid State Electron.*, vol. 53, pp. 1220–1226, 2009.

[19] D. Sun *et al.*, "Flexible high-performance carbon nanotube integrated circuits," *Nature Nano.*, vol. 6, pp. 156–161, 2011.

[20] K. Myny *et al.*, "An 8-bit, 40-instructions-per-second organic microprocessor on plastic foil," *IEEE J. Solid-State Circuits*, vol. 47, pp. 284–291, 2012.

[21] W. Lee, H. Choi, D. Kim, and K. Cho, "Microstructure dependent bias stability of organic transistors," *Adv. Mater.*, vol. 26, pp. 1660–1680, 2014.

[22] S. Na *et al.*, "Enhanced performance of inverted polymer solar cells with cathode interfacial tuning via water-soluble

polyfluorenes," *Appl. Phys. Lett.*, vol. 97, p. 223305, 2010.

[23] Y. Xue and M. Ratner, "Electron transport in semiconducting carbon nanotubes with hetero-metallic contacts," *Nanotechnol.*, vol. 16, pp. 5–9, 2005.

[24] H. Sirringhaus, "Reliability of oganic field-effect transistors," *Adv. Mater.*, vol. 21, pp. 3859–3875, 2009.

[25] S. Mathijssen *et al.*, "Dynamics of threshold voltage shifts in organic and amorphous silicon field-effect tansistors," *Adv. Mater.*, vol. 19, pp. 2785–2789, 2007.

[26] H. Yan *et al.*, "A high-mobility electron-transporting polymer for printed transistors," *Nature*, vol. 457, pp. 679–686, 2009.

[27] G. Giri *et al.*, "Tuning charge transport in solution-sheared organic semiconductors using lattice strain," *Nature*, vol. 480, pp. 504–508, 2011.

[28] A. Troisi, "Charge transport in high mobility molecular semiconductor: Classical models and new theories," *Chem. Soc. Rev.*, vol. 40, pp. 2347–2358, 2011.

[29] H. Kang *et al.*, "Fully roll-to-roll gravure partially printed wireless (13.56 MHz) sensor-signage tags for smart packaging," *Sci. Rep.*, vol. 4, no. 5387, 2014.

[30] Y. Jung, "Fully gravure printed flexible and disposable wireless cyclic voltammetry tags," Ph.D. dissertation, The Graduate School of Sunchon National Univ., Suncheon, Korea, 2014.

[31] M. Estrada *et al.*, "Accurate modeling and parameter extraction method for organic TFTs," *Solid State Electron.*, vol. 49, pp. 1009–1016, 2005.

[32] P. Kassal, I. Steinberg, and M. Steinberg, "Wireless smart tag with potentiometric input for ultra-low-power chemical sensing," *Sens. Actuators B*, vol. 184, pp. 254–259, 2013.

[33] N. Lim, J. Kim, S. Lee, N. Kim, and G. Cho, "Screen printed resonant tag for electronic article surveillance tags," *IEEE Trans. Adv. Packag.*, vol. 32, pp. 72–76, 2009.

[34] H. Koo *et al.*, "Scalability of carbon-nanotube-based thin film transistor for a flexible electronic device through an roll-to-roll gravure printing system," *Sci. Rep.*, 2014.

[35] S. Park, Y. Kim, J. Han, D. Moon, and W. Kim, "High-performance polymer TFTs printed on a plastic substrate," *IEEE Trans. Electron. Devices*, vol. 49, pp. 2008–2015, 2002.

[36] Q. Cao *et al.*, "Medium-scale carbon nanotube thin-film integrated circuits on flexible plastic substrates," *Nature*, vol. 454, pp. 495–500, 2008.

[37] T. Zaki *et al.*, "AC characterization of organic thin-film transistors with asymmetric gate-to-source and gate-to-drain overlaps," *Org. Electron.*, vol. 14, pp. 1318–1322, 2013.

[38] J. Noh *et al.*, "Integrable single walled carbon nanotube (SWNT) network based thin film transistors using roll-to-roll gravure and inkjet," *Org. Electron.*, vol. 12, pp. 2185–2191, 2011.

[39] J. Noh *et al.*, "Fully gravure-printed flexible full adder using SWNT-based TFTs," *IEEE Electron. Device. Lett.*, vol. 33, pp. 1574–1576, 2012.

[40] M. Jung *et al.*, "Roll-to-roll gravure with nanomaterials for printing smart packaging," *J. Nanosci. Nanotechnol.*, vol. 14, pp. 1303–1317, 2014.

[41] H. Kang *et al.*, "Megahertz-class printed high mobility organic thin-film transistors and inverters on plastic using attoliter-scale high-speed gravure-printed sub-5 μm gate electrodes," *Org. Elect.*, vol. 15, pp. 3639–3647, 2014.

[42] M. Pudas, N. Halonen, P. Granat, and J. Vahakangas, "Gravure printing of conductive particulate polymer inks on flexible substrates," *Prog. Org. Coat.*, vol. 54, pp. 310–316, 2005.

[43] M. Houssa, A. Stesmans, M. Naili, and M. Heyns, "Charge trapping in very thin high-permittivity gate dielectric layers," *Appl. Phys. Lett.*, vol. 77, pp. 1381–1383, 2000.

[44] Y. Park, J. Lim, H. Lee, and K. Cho, "Interface engineering in organic transistors," *Mater. Today*, vol. 10, pp. 46–54, 2007.

[45] D. Kim, S. Lee, S. Jeong, and J. Moon, "All-ink-jet printed flexible organic thin-film transistors on plastic substrates," *Electrochem. Solid-State Lett.*, vol. 12, p. H1950H197, 2009.

[46] W. Monch, *Semiconductor Surfaces and Interfaces*. Berlin, Germany: Springer-Verlag, 2001.

[47] C. Bock, D. Pham, and U. Kunze, "Improved morphology and charge carrier injection in pentacene field-effect transistors with thiol-treated electrodes," *J. Appl. Phys.*, vol. 10, p. 11517, 2006.

[48] Y. Li, X. Wang, S. Xu, and W. Xu, "The solvent effect on the luminescence of silver nanoclusters," *Phys. Chem. Chem. Phys.*, vol. 15, pp. 2665–2668, 2013.

[49] P. Lau *et al.*, "Fully printed, high performance carbon nanotube thin-film transistors on flexible substrates," *Nano Lett.*, vol. 13, pp. 3864–3869, 2013.

[50] J. Noh *et al.*, "Fully gravure printed half adder on plastic foils," *IEEE Electron. Device. Lett.*, vol. 32, no. 11, pp. 1555–1557, 2011.

[51] S. Hur, C. Kocabas, O. Park, M. Shim, and J. Rogers, "Printed thin-film transistors and complementary logic gates that use polymer-coated single-walled carbon nanotube networks," *J. Appl. Phys.*, vol. 98, p. 114302, 2005.

[52] D. Tu, L. Herlogsson, L. Kergoat, X. Crispin, and M. Berggren, "A static model for electrolyte-gated organic field-effect transistors," *IEEE Trans. Electron Devices*, vol. 58, no. 10, pp. 3574–3582, 2009.

[53] G. Ting, O. Acton, H. Ma, J. Ka, and A. Jen, "Study on the formation of self-assembled monolayers on sol-gel processed hafnium oxide as dielectric layers," *Langmuir*, vol. 25, pp. 2140–2147, 2009.

[54] D. Baron, E. Labelle, D. Coursolle, J. Gralnick, and D. Bond, "Electrochemical measurement of electron transfer kinetics by shewanella oneidensis MR-1," *J. Biol. Chem.*, vol. 284, no. 42, pp. 28865–28873, 2009.

[55] I. Oh, H. Lee, H. Yang, and J. Kwak, "Ion and water transports in Prussian blue films investigated with electrochemical quartz crystal microbalance," *Electrochem. Commun.*, vol. 3, pp. 274–280, 2001.

[56] R. Mackenzie, C. Fraschina, T. Sannomiya, V. Auzelyte, and J. Vörös, "Optical sensing with simultaneous electrochemical control in metal nanowire arrays," *Sensor*, vol. 10, pp. 9808–9830, 2010.

[57] M. Huang, Y. Ding, and X. Li, "Lead-ion potentiometric sensor based on electrically conducting microparticles of sulfonic phenylenediamine copolymer," *Analyst*, vol. 138, pp. 3820–3829, 2013.

[58] H. Falk and F. Stefano, "A basic tutorial on cyclic voltammetry for the investigation of electroactive microbial biofilms," *Chem. Asian J.*, vol. 7, pp. 466–475, 2012.

[59] T. Karl *et al.*, "Human breath isoprene and its relation to blood cholesterol levels: New measurements and modeling," *J. Appl. Phys.*, vol. 91, pp. 762–770, 2001.

[60] F. Armstrong, "Recent developments in dynamic electrochemical studies of adsorbed enzymes and their active sites," *Curr. Opin. Chem. Biol.*, vol. 9, pp. 110–117, 2005.

[61] J. Ascaso *et al.*, "Diagnosing insulin resistance by simple quantitative methods in subjects with normal glucose metabolism," *Diabetes Care*, vol. 26, pp. 3320–3325, 2003.

[62] Y. Jung *et al.*, "Fully printed flexible and disposable wireless cyclic voltammetry tag," *Sci. Rep.*, vol. 5, no. 8105, 2015.

[63] J. Ding *et al.*, "Enrichment of large-diameter semiconducting SWCNTs by polyfluorene extraction for high network density thin film transistors," *Nanoscale*, vol. 6, pp. 2328–2339, 2014.

[64] A. Zanella, N. Bui, A. Castellani, L. Vangelista, and M. Zori, "Internet of things for smart city," *IEEE Internet Things J.*, vol. 1, pp. 22–32, 2014.

ABOUT THE AUTHORS

Jinsoo Noh received the B.S., M.S., and Ph.D. degrees in electrical engineering from Chosun University, Gwangju, Korea, in 2002, 2004, and 2007, respectively.

In 2008, he was a Visiting Researcher with The University of New South Wales (UNSW), Sydney, NSW, Australia. From 2010 to 2014, he was at the Printed Electronics Research Center, Paru Corporation, Suncheon, Korea, as a Research Engineer. Currently, he is a Research Professor at Sunchon National University, Suncheon, Korea. His research interests include printed electronics, circuit design, and simulation for printed electronics.

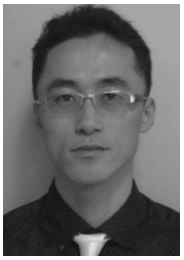

Minhoon Jung received the B.S., M.S., and Ph.D. degrees in chemical engineering from Sunchon National University, Suncheon, Korea, in 2004, 2006 and 2012, respectively.

In 2005, he joined the Printed Electronics Research Institute of Paru Corporation, Suncheon, Korea, as a Research Engineer. Currently, he is working on the commercialization of R2R gravure printed RFID tags using SWNT based TFTs.

Younsu Jung received the M.S degree in chemistry education and the Ph. D. degree in printed electronics from Sunchon National University, Suncheon, Korea, in 2009 and 2014, respectively.

Currently, he is a Research Professor in the BK21 Plus Program at Sunchon National University. His research interests include printed sensor devices based on electrochemistry and the stability of printed transistors.

Chisun Yeom received the B.S degree in chemical engineering and the M.S. degree in printed electronics in the World Class University Program from Suncheon National University, Suncheon, Korea, in 2012 and 2014, respectively.

In 2014, he joined the Regional Innovation Center for Green Technology and Advanced Materials as a Research Engineer. He is working on printed SWNT-based TFTs for CMOS logic circuits and backplanes for pressure sensor arrays using R2R and S2S gravure printing systems.

Myoungho Pyo received the B.S. and M.S. degrees from Seoul National University, Seoul, Korea, and the Ph.D. degree in conducting polymers from the University of Florida, Gainesville, FL, USA, in 1982, 1984, and 1994, respectively.

From 1984–1988, he was a Researcher at the Central Research Institute of LG Chem Ltd., Daejeon, Korea. A short postdoctoral experience, under the guidance of Prof. Allen J. Bard at the University of Texas, Austin, Austin, TX, USA, for 10 months was followed by a Professor position in the Department of Chemistry at Sunchon National University, Suncheon, Korea, in 1995. Currently, he is the head of the Printed Electronic Engineering Department, and a Director of the BK21 Plus Program and of the Advanced IT-Convergence Materials Institute. His research interests cover the development of new electrode materials, including rechargeable batteries, and the construction of flexible batteries with no strain mismatch.

Gyoujin Cho (Member, IEEE) received the Ph.D. degree from the University of Oklahoma, Norman, OK, USA, in 1995.

In 1996, he joined the faculty of the Department of Chemical Engineering, Sunchon National University, Suncheon, Korea. Currently, he is a faculty member in the Department of Printed Electronics Engineering, World Class University Program, Sunchon National University. Since 2002, he has focused his research on printed electronics and successfully demonstrated all-gravure printed 13.56 MHz RFID tags (4, 16, 32, and 96 bit). He is developing fully R2R gravure printed TFT backplane arrays for large area digital signage and wireless cyclic voltammetry tags as a platform for RF *e*-sensor based smart packaging.